Article

Analysis of the Transition of an Explosive Cyclone to a Mediterranean Tropical-like Cyclone

John Kouroutzoglou [1,2,*], Ioannis Samos [2,3], Helena A. Flocas [2,*], Maria Hatzaki [4], Christos Lamaris [1], Anna Mamara [3] and Antonios Emmannouil [3]

[1] Regional Meteorological Centre, Hellenic Tactical Air Force, 41001 Larisa, Greece; christos.lamaris@hnms.gr
[2] Sector of Environmental Physics—Meteorology, Department of Physics, National and Kapodistrian University of Athens, University Campus, 15784 Athens, Greece; ioannis.samos@phys.uoa.gr
[3] Hellenic National Meteorological Service, 16777 Athens, Greece; anna.mamara@hnms.gr (A.M.); antonis.emmanouil@hnms.gr (A.E.)
[4] Sector of Geography and Climatology, Department of Geology and Geoenvironment, National and Kapodistrian University of Athens, University Campus, 15784 Athens, Greece; marhat@geol.uoa.gr
[*] Correspondence: ioankour@phys.uoa.gr (J.K.); efloca@phys.uoa.gr (H.A.F.)

Abstract: This study investigates the dynamics of the development phases of a Mediterranean tropical-like cyclone (medicane) in the southern Ionian Sea, on 28 September 2018 that caused high impact phenomena in the central and eastern Mediterranean, focusing on the transition from explosive cyclone to medicane. The symmetry and the warm core structure of the system have been demonstrated via phase space diagrams determining three phases of the system development that are then supported on a dynamical basis. During the first phase of the system, baroclinic instability triggered the formation of the explosive cyclone, when strong upper-level PV anomalies at the dynamic tropopause level moved towards a pre-existed area of enhanced low-level baroclinicity over the coastal areas of Libya along with positive SST anomalies. The surface frontal structure was enhanced under the influence of the upper-level dynamic processes. During the second phase when the medicane formed, low-level diabatic processes determined the evolution of the surface cyclone, without any significant support from baroclinic processes in the upper troposphere. The distortion of the low-level baroclinicity and the frontal structure began after the initial weakening of the upper-level dynamics. During the third phase, the system remained barotropic, being affected by similar mechanisms as in the second phase but with lower intensity. The transition mechanism is not only the result of the seclusion of warm air in the cyclone core but, mainly, the continuation of an explosive cyclone or an intense cyclone when the occlusion began to form.

Keywords: medicanes; Mediterranean cyclones; warm core systems; explosive cyclones; cyclone dynamics

1. Introduction

The Mediterranean tropical-like cyclones, known as medicanes [1], are intense low-pressure systems that exhibit some distinct features of tropical cyclones, such as a cloud-free area at their centre (the 'eye'), spiral bands with deep convection around it, intense surface winds and a warm-core and symmetric structure [2]. They are meso-scale cyclones, with diameter, usually less than 300 km, and intensely low sea level pressure [3,4]. Medicanes form over the sea in autumn and winter, mainly in the western Mediterranean and the Ionian Sea [5], causing hazardous weather phenomena, such as strong winds, heavy precipitation and thunderstorms, tornadoes, storm surges with severe damages in properties, agriculture, communication networks and loss of human lives [6].

Previous studies have examined the dynamics of specific cases of medicanes, focusing on different aspects of their structure and evolution [7–10]. Despite their barotropic structure, medicanes seem to develop under the influence of both baroclinic and diabatic

processes [11–13]. Upper-level forcing plays an important role along with the low-level baroclinic zone [14,15] similar to other intense Mediterranean cyclones. A PV streamer or a cut-off system is commonly present close to medicanes and therefore, baroclinic forcing is expected to contribute to their development [6,14,16,17]. The diabatic processes, including convection and sea surface fluxes, play a crucial role later by sustaining or strongly driving medicanes [13]. The transition of an extratropical cyclone to medicane takes place as the cyclone undergoes warm seclusion while the warm core structure extends from the surface up to the tropopause, with its maximum below 700 hPa [12,18,19]. However, the spatial and temporal distribution of the diabatic processes can differ among different cases of medicanes [12].

The conceptual model of an extratropical cyclone presented by [20] and the fundamental principles of the above model described by [21], can be directly related to low-level non-baroclinic processes. Moreover, the recent consideration of three-dimensional airflow along organized surface frontal activities, as it is described with the aid of the conveyor belts [22–24] and the connection with the occlusion process and the warm core seclusion [25], further contribute to better explaining the physical mechanisms of cyclogenesis. The authors of [26] provided a clear picture about the role of the conveyor belts for the intensification of extratropical cyclones, employing the warm conveyor belt strength during the period of cyclone strongest deepening.

Mediterranean explosive cyclones are synoptic scale systems that form mainly over the sea, characterised by strong and rapid surface deepening with a normalized deepening rate, greater than or equal to 1 Bergeron [27–29] contrasting ordinary cyclones that do not fulfil this criterion. According to [29,30] explosive cyclones in the Mediterranean develop from baroclinic processes at upper and lower levels, interacting with diabatic mechanisms at lower levels. Despite their different structure and formation mechanisms as compared to medicanes, explosive cyclones can also cause severe impacts on Mediterranean coastal areas.

The synergy of both baroclinic and diabatic forcing is considered to contribute to the genesis of both medicanes and explosive cyclones, however, with different manner and structure. Nevertheless, the transition of an explosive Mediterranean cyclone with frontal characteristics to a tropical- like barotropic system, such as a medicane, is not yet explicitly addressed [19,31]. The model of conveyor belts can help to explain this transition, through the occlusion process, as interacting with other physical mechanisms.

The objective of this study is to investigate the dynamics of a Mediterranean cyclonic system at the upper and lower levels that initially appeared as an explosive cyclone, then transformed to a medicane, becoming eventually an intense cyclone during the last phase. More specifically, we intend to respond to the critical question of when and why the system underwent these transitions along its trajectory, based on the theoretical approach of the occluded fronts and the occlusion process in extratropical cyclone [21] complied with the conceptual model of [20].

2. Data

For this study, ERA-Interim datasets [32] on a $0.125° \times 0.125°$ regular latitude–longitude grid, interpolated from the respective spectral resolution T255 ($0.75° \times 0.75°$ km) at 6 h intervals, were employed. The examined region extends from 24° N to 64° N and from 30° W to 50° E. Analysis fields at 6-hourly intervals from 26 September 2018 00 UTC to 30 September 2018 12 UTC were selected. The data were retrieved at mean sea level, on pressure levels and isentropic levels and, on the level of the dynamic tropopause (2 PVU).

The analysis was based on the calculation of (a) spatial distributions of 850–700 hPa, 900–600 hPa and 600–300 hPa thermal wind, Q-vectors at 850 and 700 hPa, 925–850 and 700–500 hPa static stability, 850 hPa temperature advection, 850–500 hPa thickness, 500 hPa relative vorticity advection by thermal wind at 1000–500 hPa, sea surface temperature (SST) anomalies as departures from the mean value of September 2018, (b) vertical cross-sections of potential vorticity, meridional wind component and potential temperature, wet bulb

potential temperature, relative humidity and vertical velocity (ω) following the cyclonic centre, and (c) temporal variations of the vertical tilting of the cyclone centre between surface and upper isobaric levels.

To investigate the impact of weather phenomena associated with the medicane focusing on the time period before, during and shortly after its tropical-like phase, the following datasets were employed: (a) accumulated and instantaneous rain rate precipitation as estimated from H SAF products of EUMETSAT,(b) lightning data from the network of the Hellenic National Meteorological Service (HNMS), (c) High Rate Information Transmission (HRIT) data from EUMETSAT, utilizing MSG-3 satellite data of channels 1–12, on an orthographic projection disseminated on a 3 × 3 km grid for channels 1–11 and on a 1 × 1 km grid for channel 12 (HRV), and (d) data received from ASCAT instrument of EUMESAT METOP A and METOP B satellites, as well as the provided altimeter data and specifically, winds and wave height during the cyclone evolution.

The examined system formed as an explosive cyclone on 27 September 2018 at 12:00 UTC over the Gulf of Sidra, attained characteristics of a tropical-like cyclone on 28 September 2018 at 06:00 UTC over the southern Ionian Sea and then, following an eastward track, approached southern Greece as an ordinary Mediterranean cyclone. The full cyclone track is presented in Figure 1a. The temporal evolution of the mean sea level pressure (MSLP) at the centre of the system is displayed in Figure 1b. Hereafter, the date (dd) and synoptic hour in UTC (hh) in September 2018 will be indicated by the abbreviation dd/hh UTC.
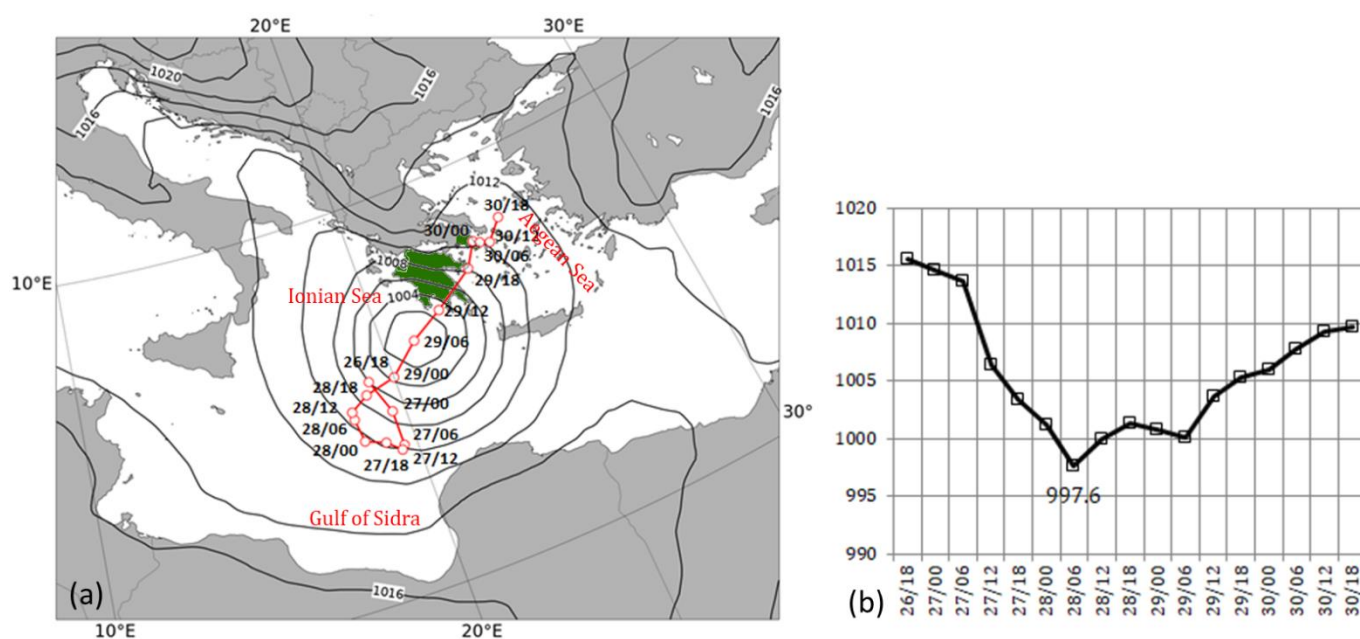

Figure 1. (**a**) System track as derived following the minimum pressure of the system from the ECMWF operational analyses. The lines are isobars at the time of medicane development at 29/06 UTC and (**b**) Temporal evolution of the mean sea level pressure at the centre of the system. The areas in green colour represent the Greek areas of the Peloponnese and Attica Peninsula that experienced the highest impact.

3. Weather Analysis

3.1. Synoptic Scale Analysis

One day before the event at 26/12 UTC, an upper-level blocking anticyclone was established over the Atlantic and Western Europe (Figure 2a), favouring an upper tropospheric downstream development on the eastern flank of the ridge which acted as a dynamically unstable ridge [33], under the effect of a strong N-NE jet streak over North Europe. The upper-level blocking extended towards Eastern Europe and the upper-level wind shifted to the N-NE sector on the eastern flanks of the dynamically unstable ridge. This shift favoured

the formation of a large-scale trough over Eastern Europe and anticyclonic disruption of the respective elongated diffluent trough [34], leading to downstream development.
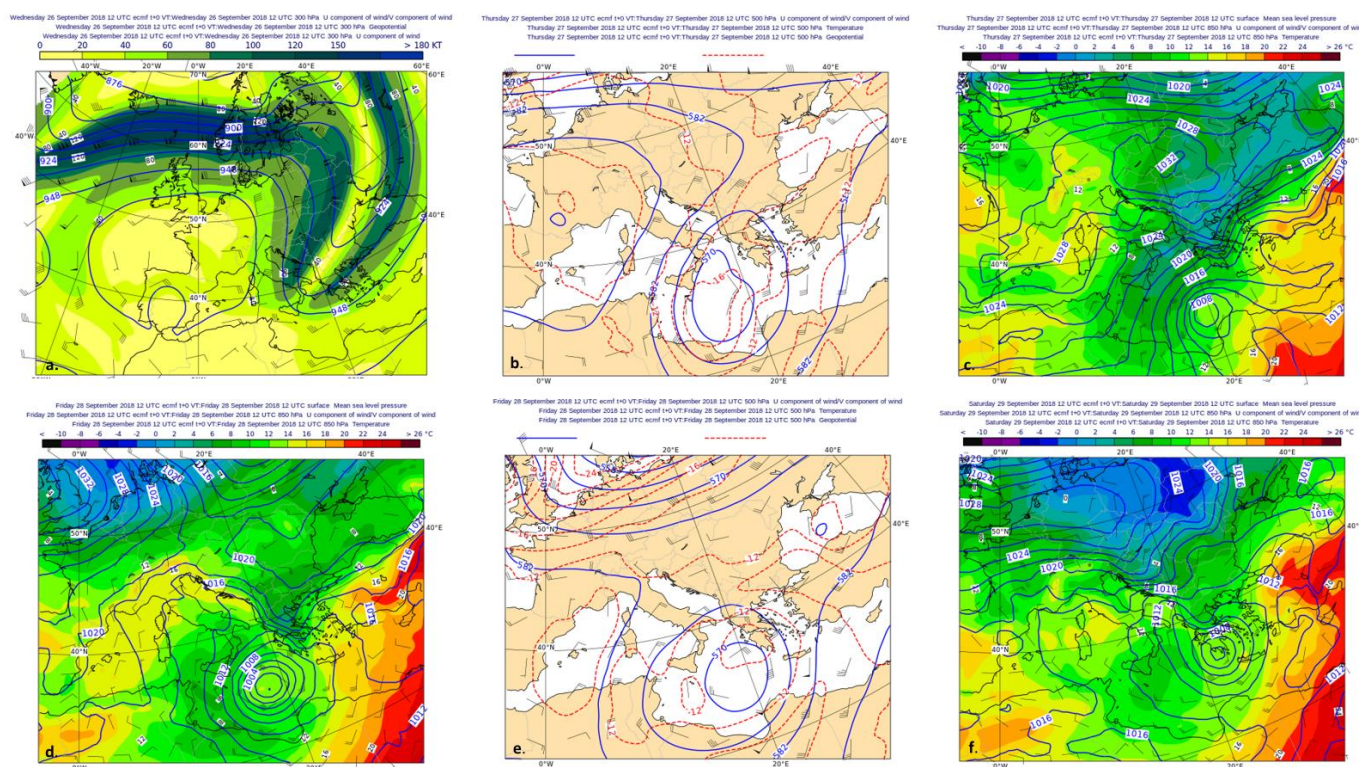

Figure 2. (**a**) 300 hPa geopotential height (continuous lines; in gpdam), isotachs (coloured areas; in knots) and winds at 26/12 UTC, (**b**) 500 hPa geopotential height (continuous lines; in gpdam), temperature (dashed lines; in °C) and winds at 27/12 UTC, (**c**) mean sea level pressure (continuous lines; in hPa), 850 hPa temperature (coloured areas; in °C) and winds at 27/12 UTC, (**d**) mean sea level pressure (continuous lines; in hPa), 850 hPa temperature (coloured areas; in °C) and winds at 28/12 UTC, (**e**) 500 hPa geopotential height (continuous lines; in gpdam), temperature (dashed lines; in °C) and winds at 28/12 UTC, and (**f**) mean sea level pressure (continuous lines; in hPa), 850 hPa temperature (coloured areas; in °C) and winds at 29/12 UTC.

Indeed, a large-scale trough that formed over the southern Adriatic Sea, propagated southwards, deepened and became a closed system over the southern Ionian Sea at 27/12 UTC (Figure 2b), is accompanied by a strong polar front jet streak and diffluent flow. This upper-level configuration along with the extension of the strong surface cold anticyclone from Central Europe towards the Greek area favoured the increase of low-level baroclinicity in the coastal areas of eastern Libya.

Surface explosive cyclogenesis occurred near the Gulf of Sidra (Figure 2c) with a surface pressure deepening of almost 16 hPa during the 12 h period between 27/12 UTC and 28/00 UTC and a central pressure of about 998 hPa at 28/06 UTC (Figure 1b), following the Capaldo and Conte (CC) mechanism [35]. The cyclone is characterised as explosive, following the criterion of [27], in terms of normalized central pressure deepening rate (NDRc) [28]. In our case, the criterion of the 12 h deepening rate was used, where the 12 h time interval was successive and overlapping every 6 h to obtain a more detailed evolution of the deepening rate of the system [36].

Then, from 28/06 UTC to 28/12 UTC, the explosive cyclone transformed to a medicane and the system remained almost stationary above the Gulf of Sidra, with no significant central pressure change (Figure 2d). The upper-level circulation continued to be characterised by a 500 hPa closed cyclone in the wider area between the southern Ionian Sea and the Gulf of Sidra (Figure 2e). Nevertheless, the transition of the upper-level circulation from a diffluent to confluent flow and the weakening of the wind maxima over the western

flanks of the upper-level cyclone, provide a clear indication of the respective weakening of the upper-level dynamics during this phase of the surface cyclone evolution, as it will be further analysed in the next section.

During the next hours, from 28/12 UTC to 29/18 UTC the surface system propagated gradually E-NE to the southern Peloponnese (southern Greece), while near hurricane-force winds and major waves hit numerous regions along its track. At 29/12 UTC, the cyclonic centre was located over Peloponnese, being gradually filled during further E-NE movement (Figure 2f). During its landfall over southern Greece from 29/12 UTC to 30/00 UTC, the system gradually beguan to decay with a central pressure of about 1004 hPa over Attica Peninsula (south-eastern Greece) at 30/00 UTC. After that, it followed an N-NE trajectory and gradually dissipated after reaching NW Turkey on 30 September.

3.2. Mesoscale Analysis

The airmass RGB satellite images show a well-developed eyewall with deep convection which obtained a spiral cloud structure and a cloud-free distinct eye between 28/00 UTC and 29/00 UTC (Figure 3a). This cloud structure began gradually dissipating after 29/12 UTC, during the cyclone's landfall in the southern Peloponnese (not shown).
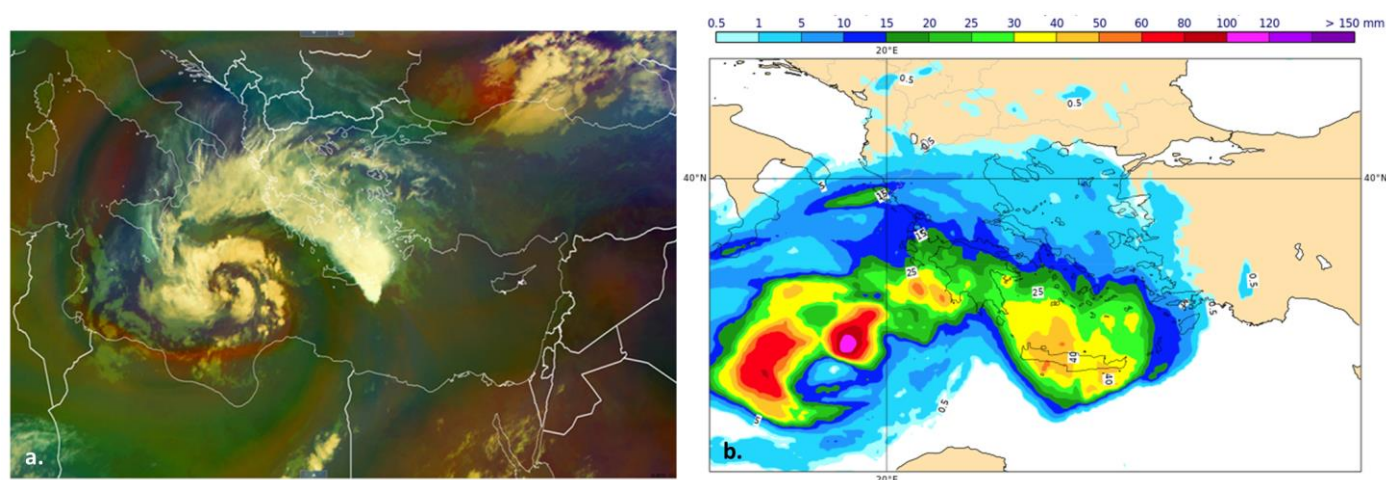

Figure 3. (**a**) AIR MASS RGB image for 28/06 UTC and (**b**) accumulated rain 24 h (mm) from 28/00 UTC to 29/00 UTC as derived by HSAP products of EUMETSAT.

The recorded values of instantaneous rainfall rate, as derived from the satellite analysis ranged between 16–19 mm/h over the area of Sidra, where the cyclone remained almost stationary until 28/12 UTC (not shown). Consistent with these measurements, the 24 h accumulated precipitation, as derived from altimetry, presented an analogous behaviour with maximum values between 100–120 mm over Sidra. Similarly, high values of accumulated precipitation affected the SW Peloponnese during the night on 28 September (100–200 mm) and the central-southern parts of Greece on 29 September when the cyclone moved eastwards from the southern Ionian Sea towards the SW Aegean Sea and the Attica region (Figure 3b). Even on 30 September, when the cyclone began dissipating, significant precipitation amounts of 60–80 mm were recorded over the eastern parts of Greece.

The altimeter recorded a maximum wave height of about 10 m over Sidra during the period 27/12 UTC–28/00 UTC and of almost 11 m in the marine area between the Peloponnese and western Crete for the period 28/00 UTC–28/12 UTC (not shown). The examination of ASCAT wind field retrievals on 27 September indicates a well-defined vortex. Furthermore, the wind field over the NE quadrant of the cyclone is enhanced with wind speeds of about 50 kts (not shown). Along with ASCAT wind retrievals, ship and METAR observations were also used to identify the marine conditions. Ships within the area of the cyclone between 27/21 UTC to 29/13 UTC, reported winds speeds up to 57 kts and ground meteorological stations up to 45 kts.

4. Objective Diagnostic of the Medicane Formation and Evolution

In order to determine objectively the time of the medicane formation and the time when the system lost the tropical-like characteristics, a mathematically defined three-dimensional phase space analysis is employed, as described by [37]. Cyclone phase is described using (a) the B parameter representing the thickness asymmetry (symmetric/non-frontal versus asymmetric/frontal) and (b) the scaled thermal wind magnitude $-V_T^L$ at the lower layers and $-V_T^U$ at the upper layers being defined by the vertical derivative of horizontal height gradient representing the cold- versus warm-core structure of the system. Thus, a cyclone life cycle can be analysed within this phase space, providing substantial insight into the cyclone structural evolution.

More specifically, the value of B at a specific atmospheric layer is defined as the difference of the mean thickness between the right and the left side (right minus left) of a cyclone relative to its motion in the lower troposphere. The location of the cyclone centre is identified by the lowest MSLP value and then the cyclone track for each following hour is estimated according to [37]. The left- and right-side mean thickness is calculated considering a circle with a radius of 200 km around the cyclone centre. Small values of B (<10 m) correspond to a thermally symmetric system without frontal activities, such as a tropical-like cyclone.

The scaled thermal wind magnitude parameters are defined as:

$$\frac{\partial(\Delta Z)}{\partial lnp}\bigg|_{900\ hPa}^{600\ hPa} = -\left|V_T^L\right| \cong \frac{\Delta Z_{600} - \Delta Z_{900}}{ln600 - ln900} \tag{1}$$

$$\frac{\partial(\Delta Z)}{\partial lnp}\bigg|_{600\ hPa}^{300\ hPa} = -\left|V_T^U\right| \cong \frac{\Delta Z_{300} - \Delta Z_{600}}{ln300 - ln600} \tag{2}$$

where ΔZ is the difference between a maximum and minimum value of geopotential height at the specific isobaric level within the employed circle with a radius of 200 km around the minimum MSLP of the low every 6 h. The warm core system is defined when $-V_T^L > 0$, $-V_T^U > 0$ and cold core when $-V_T^L < 0$, $-V_T^U < 0$.

Although a radius of 500 km was chosen for the study of tropical cyclones by [37], in this work the radius of 200 km was considered most suitable, considering that Mediterranean tropical-like cyclones have a smaller size than tropical cyclones and a possible choice of a larger radius would smooth out the characteristics of the Mediterranean cyclones [38,39]. However, sensitivity tests were also performed (not shown) for smaller radius (100 and 150 km) and for larger radius (350 km) without significant differences in the cyclone's structure and evolution.

The atmospheric levels below 900 hPa were not included in the calculation of the above-mentioned parameters to avoid extrapolation below ground or within the boundary layer. The atmospheric levels above 300 hPa were excluded to prevent the presence of the stratospheric phase, which is often the opposite of the tropospheric phase. Therefore, for the specification of cyclone's characteristics, the lower troposphere is represented by the layer 900–600 hPa and the upper troposphere by the layer 600–300 hPa, following the methodology used in previous studies [2,37,38,40].

Since a medicane is a symmetric cyclone with a deep warm-core structure, similarly to a tropical cyclone, the parameter B should be less than 10 and both $-V_T^L$ and $-V_T^U$ should be positive.

According to Table 1, where the parameters B, $-V_T^L$, and $-V_T^U$ are demonstrated every 6 h, the system was clearly cold core during the stage of explosive cyclogenesis from 27/06 UTC to 27/18 UTC, although exhibited a symmetrical structure. The warm-core structure began forming at 28/00 UTC at lower levels after the formation of the well-defined occlusion processes, following the conceptual model of [20]. From 28/06 UTC to 28/12 UTC, a deep warm core symmetric structure was evident throughout the troposphere, implying the transition to a tropical-like Mediterranean cyclone. From 28/18 UTC to 29/12 UTC, the cyclone remained warm core at low and upper levels, however, it

lost its symmetry. After 30/00 UTC, the system did not have the structure of a medicane and attained characteristics of an extratropical cyclone (not shown).

Table 1. Temporal variation of 600–900 hPa thermal wind ($-V_T^L$), 300–600 hPa thermal wind ($-V_T^U$) and parameter B for the layer 600–900 hPa at a radius of 200 km around the centre of the minimum SLP every 6 h. Green colour indicates symmetry and red colour warm-core system.

Parameter	Layer (hPa)	27/06	27/12	27/18	28/00	28/06	28/12	28/18	29/00	29/06	29/12	29/18
B	600–900	−2.7	−37.7	1.9	2.3	5.2	7.0	13.0	12.0	14.0	15.0	11.0
$-|V_T|$	300–600	−141.8	−143.8	−65.9	−17.8	43.4	50.5	41.6	34.6	46.9	64.3	48.5
	600–900	−44.4	−25.6	−4.1	86.8	95.8	32.6	24.0	−5.5	44.3	10.7	−3.9

The slope of the vertical profile of ΔZ at 27/06 UTC and 27/12 UTC in Figure 4a,b also suggests a cold-core cyclone within the layers of 600–900 hPa and 300–600 hPa, complying with the negative values of $-V_T^L$ and $-V_T^U$ during this period (see Table 1), and the greater magnitude of $-V_T^U$ [35]. After 27/18 UTC (Figure 4c,d), a gradual reversal of the sign of the slope of ΔZ was found, representing a warm core structure both for 600–900 hPa and 300–600 hPa layers, in accordance with the positive values of $-V_T^L$ and $-V_T^U$ and the greater magnitude of $-V_T^L$ [35].
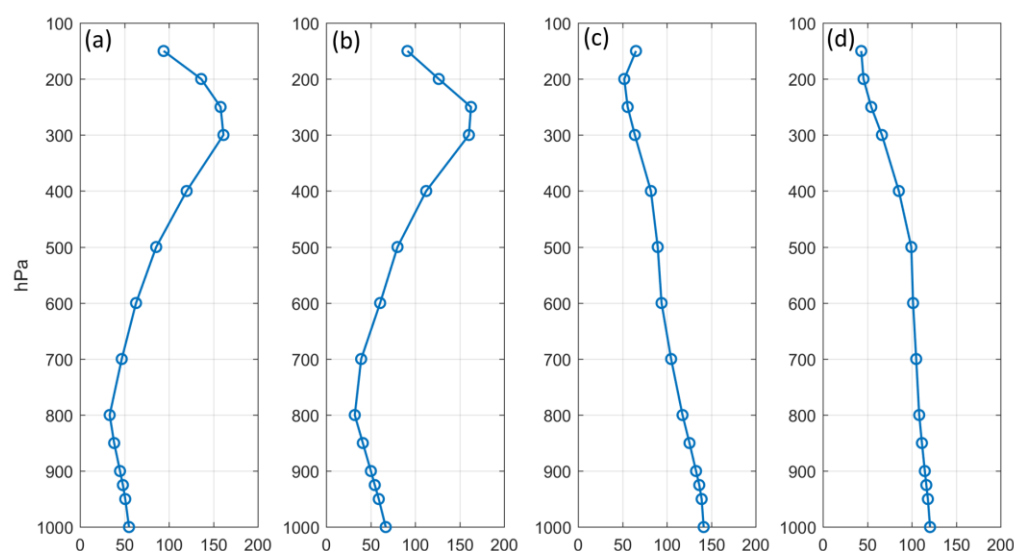

Figure 4. Temporal variation of the vertical profile of ΔZ (i.e., the difference between maximum and minimum value of geopotential height at a specific isobaric level within the employed circle with a radius of 200 km) at (**a**) 27/06 UTC, (**b**) 27/12 UTC, (**c**) 28/06 UTC, and (**d**) 28/12 UTC.

5. Dynamic Analysis

According to the analysis in previous sections, the following phases of the system development can be identified: The first phase (27/00 UTC–28/00 UTC) refers to the explosive deepening of the cyclone, the second phase (28/06 UTC–28/12 UTC) to the formation of the medicane and the third phase (28/18 UTC–29/18 UTC) to the transformation to an intense midlatitude cyclonic system.

5.1. First Phase

During the first phase, the high values of the 600–300 hPa thermal wind (Figure 5a) imply an increase in the upper-level baroclinicity that contributes to the surface explosive deepening. It should be noted that the maximum of the 600–300 hPa (Figure 5a) and 700–500 hPa (not shown) thermal wind propagated southwards towards the Gulf of Sidra from 25/12 UTC to 26/18 UTC, following the upper-level trough. At 27/00 UTC, this maximum was found over the area of surface explosive cyclogenesis. After 28/06 UTC,

the upper-level thermal wind decreased. Within this baroclinic environment, a westward tilting of the system was apparent with height during the first phase, mainly between the 500 and 300 hPa isobaric levels (Figure 6a) which gradually decreases implying the gradual transition to an upper-level symmetrically thermal structure.
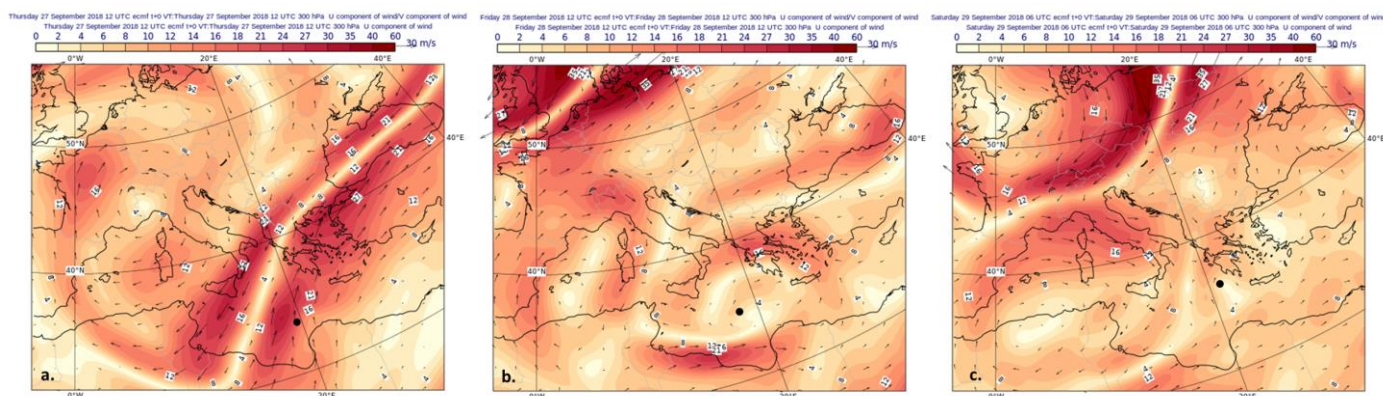

Figure 5. Thermal wind at 600–300 hPa for (**a**) 27/12 UTC, (**b**) 28/12 UTC, and (**c**) 29/06 UTC. Coloured areas denote the magnitude and the vectors the direction of thermal wind. Black dot indicates the location of the system centre.
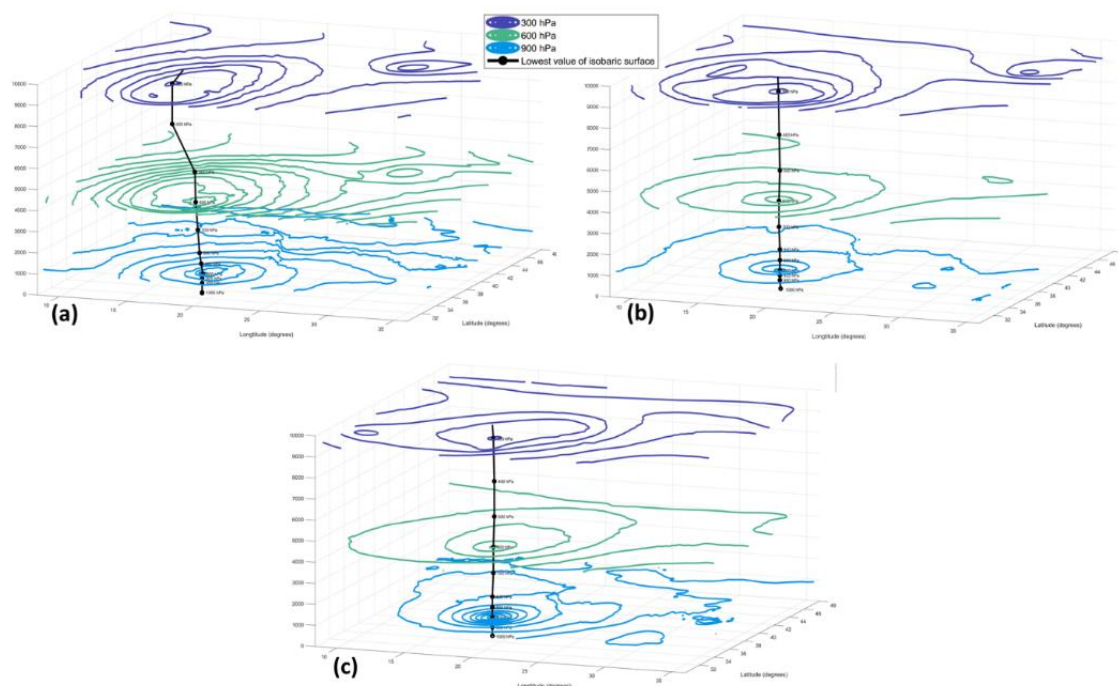

Figure 6. Three-dimensional representation of the geopotential height distribution around the cyclone centre at 900 hPa (light blue), 600 hPa (green) and 300 hPa (dark blue) at (**a**) 27/18 UTC, (**b**) 28/06 UTC, and (**c**) 28/18 UTC. Black dots represent the minimum value of geopotential height at each isobaric level and black line represents the vertical tilt with height (in meters).

In order to investigate the changing relationship between the main area of upward motion and the centre of depression during cyclone development, the relative vorticity advection at 500 hPa by the thermal wind for the layer 1000–500 hPa [41] is examined in Figure 7. During the first phase, a maximum of the positive vorticity advection is evident in the northwest of the surface cyclone at 27/12 UTC, while enhanced 1000–500 hPa thermal wind complies with this positive vorticity advection [42] towards the area of surface development (see Figure 7a), enhancing the upward motion. Furthermore, the

1000–500 hPa thickness decreases above the surface cyclone, which in turn decreases the geopotential tendency and intensifies the upper-level trough. Thus, both vorticity and thermal advection terms present a well developing baroclinic system.
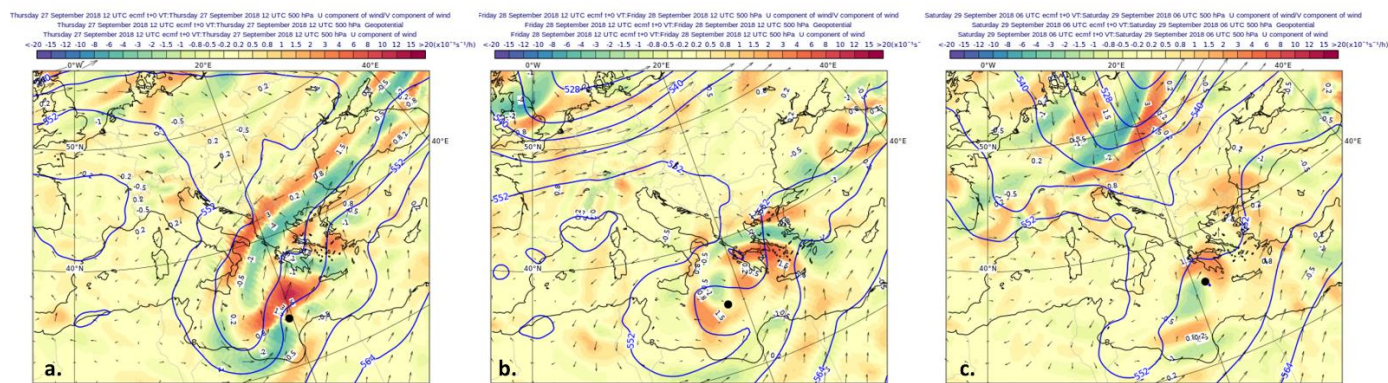

Figure 7. Relative vorticity advection at 500 hPa by the 1000–500 hPa thermal wind at (**a**) 27/12 UTC, (**b**) 28/12 UTC, and (**c**) 29/06 UTC. The contours represent the 1000–500 hPa thickness, the coloured area the relative vorticity advection and the vectors the 1000–500 hPa thermal wind. Black dot on the maps indicates the location of the system centre.

Moreover, the distributions of PV on 315 K (Figure 8a) exhibited an extended PV streamer that represents the equatorward intrusion of stratospheric high potential vorticity air (see also Figure 3b), and a cold tropopause anomaly upstream the surface cyclogenesis on 27 September, which further contributed to the explosive deepening [42]. In fact, a PV streamer is identified in Figure 8a, which is a pattern which favours the formation of Mediterranean cyclones [17]. The cross-section of the meridional wind component, potential temperature, and PV along the constant-latitude 33.5° N at 27/12 UTC (Figure 9a), following the surface cyclone centre, verifies this deep intrusion of the stratospheric air in the troposphere to the level of 500 hPa and a cold-core structure with isentropes bending upwards below 500 hPa. It is apparent that the high-PV air descended at low latitudes (33.5° N–15° E) at the PFJ flanks, interacting with the low-level baroclinicity over the African continent. Thus, the upper-level dynamics during the first phase are favourable for the development of an explosive cyclone in conjunction with the low-level baroclinicity [43].
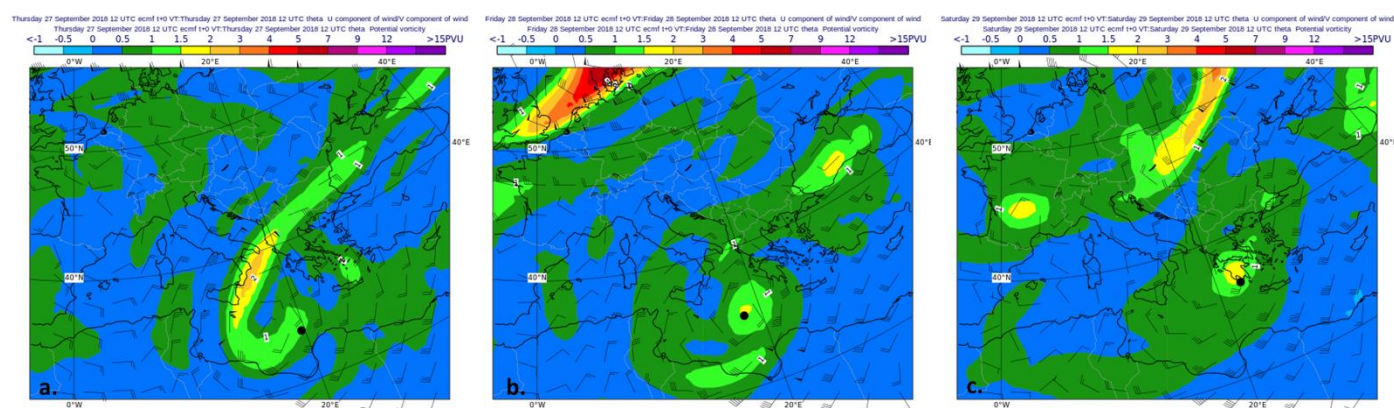

Figure 8. PV distribution on the isentropic level 315 K at (**a**) 27/12 UTC, (**b**) 28/12 UTC, and (**c**) 29/12 UTC. Black dot on the maps indicates the location of the system centre.

At low levels, cold-air advection occurred from the northern parts of the central and the eastern Mediterranean (not shown), following the extension of the cold anticyclone over the Balkans and the wind shift of low-level winds to an N–NE direction. Therefore, a strong baroclinic zone formed near the cyclonic centre over the coastal parts of Libya on

27/12 UTC, resulting from the interaction of the cold air with the pre-existed warmer air over the respective southern maritime/coastal areas. This baroclinic zone is manifested in the vertical cross-section of Figure 9a at 33.5° N, 20° E near the cyclonic centre and verified by the enhanced values of thermal wind 850–700 hPa (not shown). Slightly positive values of static stability (not shown) were found over the coastal areas of Libya for 27/12 UTC, with a slight decrease compared to the 300–500 hPa layer, indicating a decrease of stratification with height. During the transition of the explosive cyclone to medicane an erosion of the upper-level PV anomaly was observed following the results of [17]. This behaviour is consistent with the necessity of low-level air with high θ*e* values for strong latent heating and cross-isentropic upward transport [17].
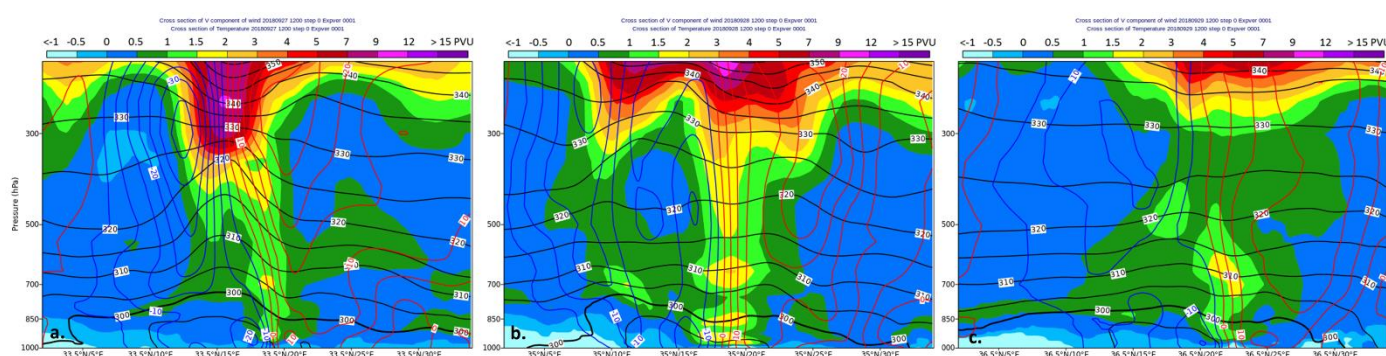

Figure 9. Longitudinal cross-sections of PV, potential temperature θ and meridional wind component following the cyclonic centre at (**a**) 27/12 UTC on 33.5° N, (**b**)28/12 UTC on 35°N, and (**c**) 29/12 UTC on 36.5° N.

In Figure 10, the Q-vectors at 700 hPa direct towards the warm air of the low-level baroclinic zone with increasing magnitude, indicating the existence of organised surface frontal activity during the first phase of the explosive development. Furthermore, the distribution of Q-vectors reveals convergence from 27/00 UTC to 28/00 UTC over the easternmost parts of the Gulf of Sidra and the NW Libyan coasts and, therefore, ascending motion.
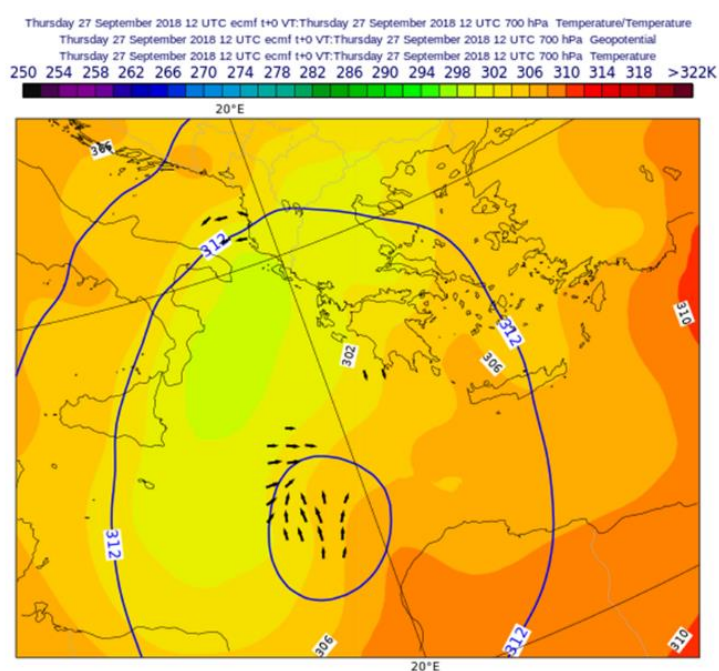

Figure 10. Q-vectors (units s^{-3} and scaling $\times 10^{11}$), potential temperature (coloured areas; in K), and geopotential height (continuous lines; in gpdam) at 700 hPa for 27/12 UTC.

The sea surface temperature (SST) between the Gulf of Sidra and the Libyan coasts varied between 26–28 °C, one day before the onset of the explosive deepening at 26/06 UTC (not shown) and remained as high as 26–27 °C during the explosive cyclogenesis at 27/12 UTC (Figure 11a). In association with the strong cold-air advection occurring over the Mediterranean, the warm sea surface enhanced the air-sea interaction and the respective turbulent sea surface fluxes [44], resulting in a significant enhancement of evaporation (i.e., transfer of energy from the sea to the atmosphere) (Figure 12a) after 26/12 UTC over the Central Mediterranean, contributing to the surface explosive deepening.
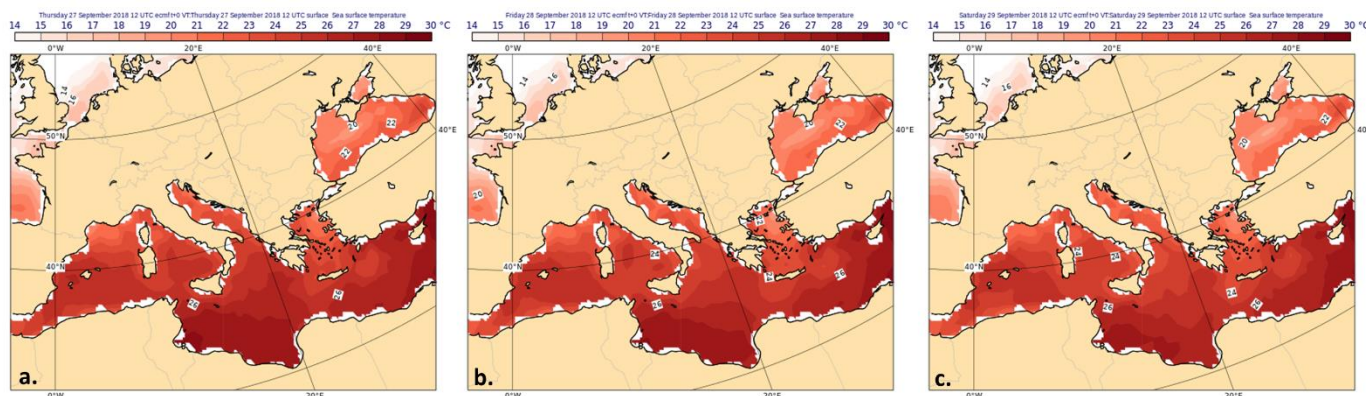

Figure 11. Sea surface temperature (SST; in °C) for (**a**) 27/12 UTC, (**b**) 28/12 UTC, and (**c**) 29/12 UTC.
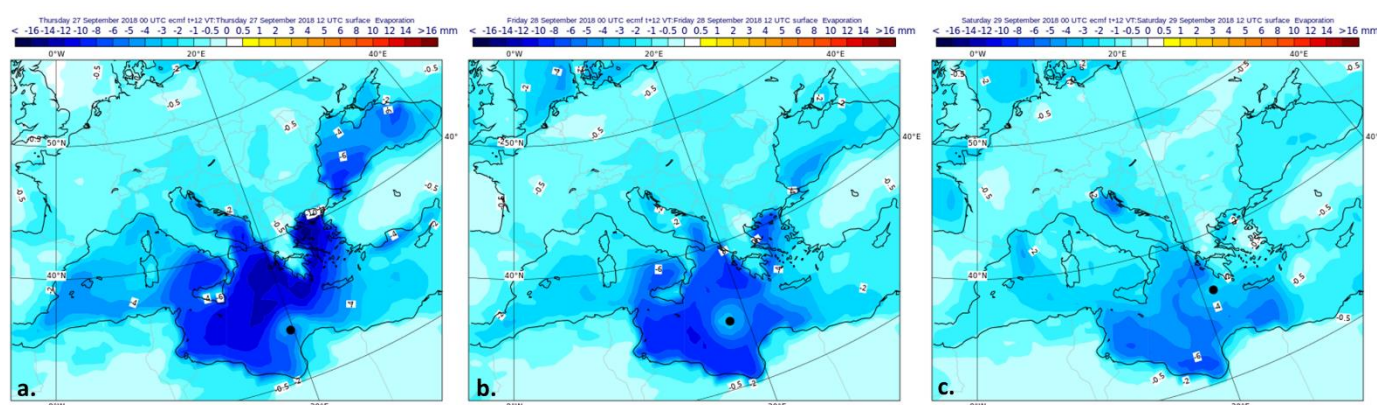

Figure 12. Twelve hour accumulated evaporation (in mm of water equivalent) (**a**) 27/00–27/12 UTC, (**b**) 28/00–28/12 UTC, and (**c**) 29/00–29/12 UTC. The evaporation is represented by negative values, denoting transfer of energy from the surface to the atmosphere. Black dot on the maps indicates the location of the system centre.

During the first phase, a first indication of the existence of the Warm Conveyor Belt (WCB) is provided by the distributions of isobars on the isentropic levels of 315 and 300 K (not shown), where isobars cyclonically turn towards the upper-level closed cyclone centre [21], advecting larger pressures from the eastern Libyan westwards via the E-SE flow. Considering that the isentropic level of 315 K corresponds to 500 hPa isobaric level in midlatitudes and the respective isentropic surface of 300 K approximately to the 850 hPa level, both distributions demonstrate the zone of ascent poleward and upward, ahead of the cold front [21,45,46].

To further elaborate this evidence, the vertical cross-sections of wet-bulb potential temperature, vertical velocity (omega), relative humidity and winds at 27/12 UTC (Figure 13a) were examined providing a picture for the existence of a well-defined WCB ahead of the cold front. Indeed, a pronounced zone of ascent is evident between 20° E–25° E, with a relative humidity of about 90%. Furthermore, a cyclonic wind shift in the lower troposphere up to about the 800 hPa isobaric level became evident, while a respective anticyclonic

wind shift formed in the layer 700–300 hPa [45,47]. The wet-bulb potential temperature θw increased with height forming a warm tongue from the lower to the upper levels.
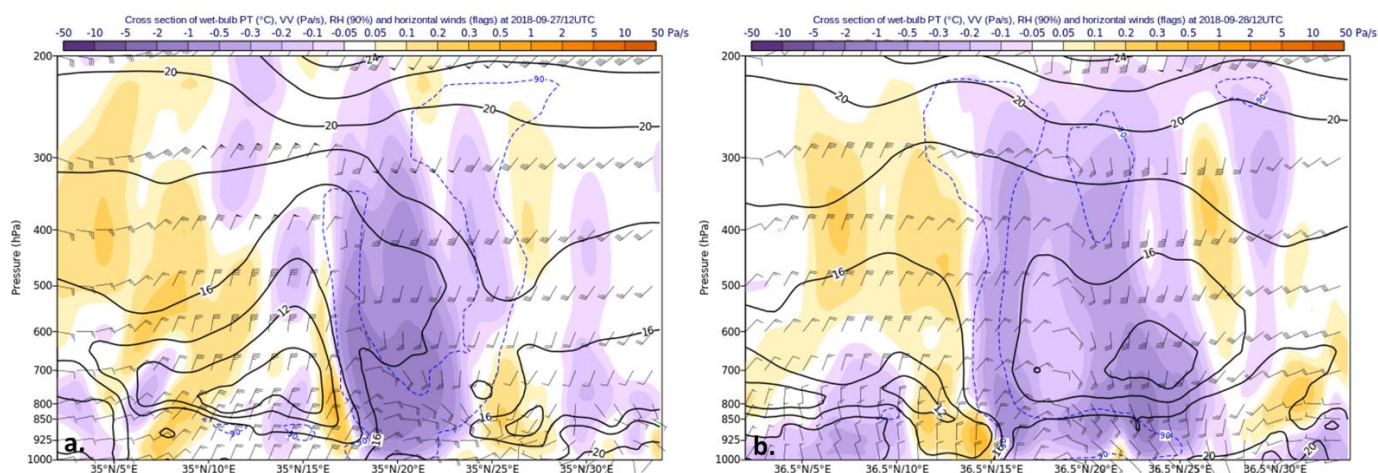

Figure 13. Cross-sections of wet-bulb potential temperature (isopleths), vertical velocity (ω) (coloured areas, in Pa/s, and horizontal wind (flags) following the cyclonic centre at (**a**) 27/12 UTC and (**b**) 28/12 UTC. Dashed blue lines represent the relative humidity value of 90%.

At the same time (27/12 UTC), the depiction of potential temperature, relative humidity, and winds (Figure 14a–c) demonstrates the intrusion of dry air descending from the upper level, the so-called dry airstream behind the cold front [21,25]. The dry airstream descended southwards to the Gulf of Sidra and intruded from the south into the cut-off low-level warm and moist air. The dry airstream was depicted on the satellite image at the same time (Figure 14d). Since the warm and moist air in the lower troposphere was combined with cold air in the upper troposphere, ascending motion was caused, and release of potential instability was favoured [25]. Thus, two out of the three components (WCB and dry airstream) of the conceptual model described analytically in [45], supported the dynamic mechanisms within the bent back structure of the cold front [20,48] and contributed to the formation of the warm seclusion [19].

Following the formation of the WCB, the distribution of the wet-bulb potential temperature θw at 27/12 UTC (not shown) presented a strong horizontal gradient in the Gulf of Sidra, connecting the diabatic heating with the existence of a WCB [23]. The θw values within the warm sector, the bent back structure of the cold front and, finally, the warm seclusion temperature values ranging between 18–20 °C—that exceeds the threshold proposed for mid-latitude extratropical cyclogenesis—indicate that a frontal depression was formed with organized WCB in the above area during the first phase [45,47].

The identification of the WCB associated with the frontal activity in accordance with the low-level PV anomaly seen in Figure 9 during the first phase, further supports the relationship between the intense diabatic heating and the well-defined WCB [24,48]. Moreover, the gradual erosion of the upper-level potential vorticity anomaly due to the intrusion of diabatic heating in the mid-troposphere [48,49], is also evident in Figure 9.

5.2. Second Phase

After the explosive cyclogenesis, the upper-level structure during the second phase pictures the transition of the explosive cyclone into a medicane through the gradual weakening of the mid- and upper-level dynamic forcing. The upper-level diffluent cyclonic flow during the first phase (Figure 2b) turned into a confluent flow with the maximum 500 hPa wind occurring on the eastern flanks during its southward propagation (Figure 2e). This confluent flow denotes a decrease of the mean absolute vorticity and a tendency of weakening of the upper-level cyclonic circulation [50].
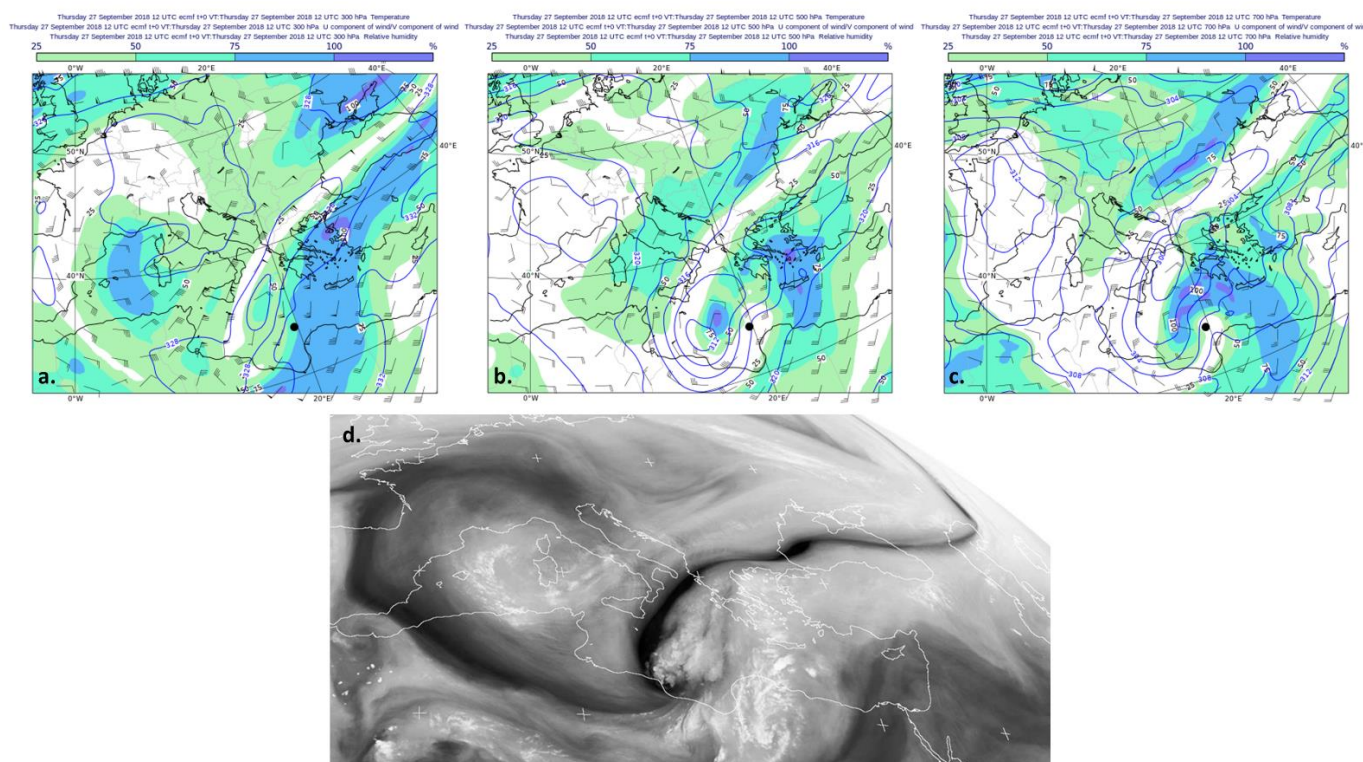
Figure 14. Potential temperature (continuous lines; in K), relative humidity (coloured contours; in %) and winds for 27/12 UTC at (**a**) 300 hPa, (**b**) 500 hPa, (**c**) 700 hPa, and (**d**) water vapor MSG (6.2 μm, channel 5) satellite image at 27/12 UTC. Black dot on the maps indicates the location of the system centre.

After 28/00 UTC, the potential vorticity on 315 K (Figure 8b) presents a different structure as compared to the first phase: the PV exhibited a cut-off maximum vertically aligned over the surface cyclone centre (see Figure 2d) with weaker values compared with the first phase, further indicating a weakening of the upper-level forcing. This structure was also found by [17] with the aid of the ECMWF Integrated Forecasting System for the same case.

Further affirming this indication during the second phase, it was found that no significant vorticity advection occurred, while 1000–500 hPa thermal wind has significantly reduced (Figure 7b), suggesting that the vertical wind shear decreases and mid- and upper-level baroclinicity vanished. Indeed, the westward tilting with height gradually weakened and at 28/06 UTC, when the medicane had been already formed, no tilting was present (Figure 6b). This is also supported by the cross-section along the constant-latitude 35° N at 28/12 UTC (Figure 9b), where the upper-level PV anomaly was vertically aligned over the surface cyclonic centre. Furthermore, no bending of the isentropes towards the upper levels is observed, indicating that upper-level cold air intrusion tends to diminish.

The absence of Q-vectors at 700 hPa (not shown) reveals the distortion of the frontal structures and the transition into a vortex with barotropic character in accordance with Figure 6b.

During the second phase, the SST retained high values in the southern Mediterranean coasts but decreased to 25 °C in the Ionian Sea (Figure 11b). Evaporation along with sensible and latent heat fluxes began to gradually weaken. Nevertheless, the contribution of the fluxes to the formation of the medicane was still significant, being reflected in the development of a low-level PV anomaly just above the cyclonic centre, peaking at 850 hPa (Figure 9b). This low-level anomaly attained its maximum value of 2 PVU at 28/12 UTC when the medicane acquired a symmetric deep warm-core structure.

Concerning the evolution of the WCB, the vertical cross-section of potential wet bulb temperature θw and vertical velocity (Figure 13b) reveals a movement of the WCB

eastwards, while the θ*w* isopleths form a cut-off area with warm-core structure in the layers between 850–450 hPa, suggesting a distortion of WCB. This is attributed to the decrease of the advection from the eastern Libyan towards the cyclone centre that was apparent during the first phase. Moreover, above the cyclone centre there is an extended barotropic cyclonic circulation throughout the troposphere. Consistent with the vertical structure, the horizontal distribution of θ*w* further supports the bent back structure of the cold front that leaded to the formation of the warm seclusion.

5.3. Third Phase

During the third phase, upper-level stratification presented a similar structure with the second phase, suggesting that the upper-level dynamic processes did not rejuvenate and did not contribute to the transformation of the medicane to an intense cyclone. More specifically, the system continued to be barotropic since no vertical tilting with height was apparent (Figure 6c). The vertical distribution of PV, potential temperature θ and meridional wind component resembled the structure of the second phase while the upper-level positive potential vorticity anomaly was confined above the 300 hPa level (Figures 8c and 9c). Similarly, the 500 hPa vorticity advection and the thickness distributions (Figure 8c) suggest the absence of upper-level baroclinic forcing (Figure 7c).

The low-level dynamic environment retained diabatic elements, responsible for the intensity of the system, despite the loss of the symmetric and deep warm core structure. More specifically, maxima of low-level PV between 0.8–1.0 PVU of diabatic origin were found in the area between the southern Ionian Sea, the Peloponnese, and the southwestern Aegean Sea (see Figure 9c). Furthermore, although surface turbulent heat fluxes and evaporation (Figure 12c) weakened, their influence affected the cyclone's evolution until the 29/18 UTC over the eastern Mediterranean along the track of the system.

It is worth mentioning that the low-level convergence between the strong low-level south-eastern flow over southern Greece and the respective north-eastern flow over the central and northern parts, strengthened again the low-level baroclinicity along with the influence of orography over continental Central and South Greece, as it is also reflected in the 850–700 hPa thermal wind distribution, until 30/00 UTC (not shown). The WCB structure had completely diminished during the third stage (not shown).

6. Discussion and Conclusions

Although previous studies have presented different approaches regarding the genesis and the dynamic characteristics of medicanes, it seems that ambiguities regarding the physical mechanisms triggering their formation remain. Ref. [19] suggested that the deep warm core in a tropical-like system is mainly an effect of the seclusion of warm air in the cyclone core. In our study, we examine this mechanism in a case of Mediterranean explosive cyclogenesis that transformed to a medicane and then to an intense cyclone during 27–29 September 2018, employing the conceptual model of cyclogenesis presented by [20] and the theory of the occlusion process by [21].

The entire analysis was performed considering three discrete phases of the cyclone evolution. These phases were defined with the aid of the Hart phase diagrams [35] but then were verified on a dynamical basis. During the first stage of explosive cyclogenesis in the Gulf of Sidra, one of the primary targets was the effective identification of the baroclinic structure of the cyclone, not only at the upper but mainly at the lower levels and the specification of surface frontal activities. With the analysis of various dynamic parameters, it was found that the surface system exhibited a well-organised baroclinic character that, however, interacted with the low-level diabatic processes, as was demonstrated in previous studies of explosive cyclogenesis in the Mediterranean [27,28].

During the second phase, it was demonstrated that the explosive frontal depression indeed transformed into a medicane. The air-sea interaction and latent heat release provided the available potential energy for further surface deepening. Even the upper-level PV anomaly did not act as a baroclinic element since it was located exactly above the surface

cyclone centre without any vertical tilting. In fact, this anomaly can be interpreted, as a mechanism favouring the vertical shrinking at the dynamic tropopause level to balance the continuous low-level vertical stretching [51].

During the third phase and the cyclone's landfall over the Peloponnese (in southern Greece), the low-level dynamic environment retained diabatic elements, responsible for the intensity of the system, despite the loss of the symmetric and deep warm core structure. The upper-level environment did not present any significant change compared to the second phase. Moreover, the low-level convergence between the strong low-level SE flow over southern Greece and the respective NE flow over the central and northern parts strengthened the low-level baroclinicity. Nonetheless, after 29/18 UTC, turbulent heat fluxes started to weaken and thus, the cyclone began gradually dissipating during its landfall over the western coastal areas of Turkey.

One of the main aspects of the Shapiro and Keyser model [20] which is also a common experience in synoptic meteorology is the fact that the deeper a cyclone is, the more organized is the bent back structure of the cold front, the so-called "T bone" [19,21] and the wrapping up and lengthening of the warm-air tongue as a result of deformation and rotation around the low centre. Thus, an explosive depression is one of the potential candidates for undergoing a transition into a medicane.

This aspect was the driver of our approach in this work. Different dynamic parameters were used to prove the occurrence of organized frontal activities and specifically the occurrence of an organized cold front during the first stage of the cyclone's propagation. Then, specific attention was given to prove the occurrence of an organized warm conveyor belt and of the dry airstream to the rear of the cold front covered. Following this approach, we demonstrated that the cut-off warm and moist air at the low levels within the cyclone centre was surrounded by dry air in the mid-troposphere favouring a vertical stratification of potential instability during the first phase. This process, related to the beginning of the occlusion process of the explosive depression, led to the formation of a low-level warm-core structure within the cyclone centre and then to a deep warm-core symmetric structure when the upper-level dynamic processes were significantly reduced, and the air-sea interaction continued to provide the cyclone with the available potential energy. We found that the identification of an organized WCB related to the frontal activity, although it was connected to the baroclinic character of the cyclone during the first phase, can also be considered as a procedure that enhanced the diabatic processes [24].

This approach allows us to implement the theoretical findings of previous studies to expand the study of the Mediterranean explosive cyclone development mechanisms, after the initiation of the occlusion process. Therefore, the transition mechanism is not only the result of the seclusion of warm air in the cyclone core but, mainly, the continuation of an explosive cyclone or an intense cyclone when the occlusion begins to form. Thus, it would be challenging to explore on a climatological basis, the possible spatial and temporal connection between Mediterranean explosive cyclogenesis or intense cyclogenesis in general and the formation of Mediterranean tropical-like cyclones and this will be the subject of future work.

Author Contributions: Conceptualization, J.K. and H.A.F.; data curation, A.M. and A.E.; investigation, J.K. and I.S.; methodology, J.K. and H.A.F.; resources, A.M. and A.E.; software, I.S. and C.L.; supervision, H.A.F.; visualization, C.L.; writing—original draft, J.K., H.A.F. and M.H.; writing—review and editing, J.K., H.A.F. and M.H. All authors have read and agreed to the published version of the manuscript.

Conflicts of Interest: The authors declare no conflict of interest.

References

1. Emanuel, K. Genesis and maintenance of "Mediterranean hurricanes". *Adv. Geosci.* **2005**, *2*, 217–220. [CrossRef]
2. Miglietta, M.M.; Mastrangelo, D.; Conte, D. Influence of physics parameterization schemes on the simulation of a tropical-like cyclone in the Mediterranean Sea. *Atmos. Res.* **2015**, *153*, 360–375. [CrossRef]
3. Businger, S.; Reed, R.J. Cyclogenesis in Cold Air Masses. *Weather Forecast.* **1989**, *4*, 133–156. [CrossRef]
4. Walsh, K.; Giorgi, F.; Coppola, E. Mediterranean warm-core cyclones in a warmer world. *Clim. Dyn.* **2014**, *42*, 1053–1066. [CrossRef]
5. Vara, A.; Gutiérrez-Fernández, J.; González-Alemán, J.J.; Gaertner, M.Á. Characterization of medicanes with a minimal number of geopotential levels. *Int. J. Climatol.* **2021**, *41*, 3300–3316. [CrossRef]
6. Nastos, P.T.; Karavana Papadimou, K.; Matsangouras, I.T. Mediterranean tropical-like cyclones: Impacts and composite daily means and anomalies of synoptic patterns. *Atmos. Res.* **2018**, *208*, 156–166. [CrossRef]
7. Pytharoulis, I.; Craig, G.C.; Ballard, S.P. The hurricane-like Mediterranean cyclone of January 1995. *Meteorol. Appl.* **2000**, *7*, 261–279. [CrossRef]
8. Homar, V.; Romero, R.; Stensrud, D.J.; Ramis, C.; Alonso, S. Numerical diagnosis of a small, quasi-tropical cyclone over the western Mediterranean: Dynamical vs. boundary factors. *Q. J. R. Meteorol. Soc.* **2003**, *129*, 1469–1490. [CrossRef]
9. Moscatello, A.; Miglietta, M.M.; Rotunno, R. Numerical Analysis of a Mediterranean "Hurricane" over Southeastern Italy. *Mon. Weather Rev.* **2008**, *136*, 4373–4397. [CrossRef]
10. Miglietta, M.M.; Moscatello, A.; Conte, D.; Mannarini, G.; Lacorata, G.; Rotunno, R. Numerical analysis of a Mediterranean 'hurricane' over south-eastern Italy: Sensitivity experiments to sea surface temperature. *Atmos. Res.* **2011**, *101*, 412–426. [CrossRef]
11. Carrió, D.S.; Homar, V.; Jansa, A.; Romero, R.; Picornell, M.A. Tropicalization process of the 7 November 2014 Mediterranean cyclone: Numerical sensitivity study. *Atmos. Res.* **2017**, *197*, 300–312. [CrossRef]
12. Miglietta, M.M.; Rotunno, R. Development mechanisms for Mediterranean tropical-like cyclones (medicanes). *Q. J. R. Meteorol. Soc.* **2019**, *145*, 1444–1460. [CrossRef]
13. Flaounas, E.; Gray, S.L.; Teubler, F. A process-based anatomy of Mediterranean cyclones: From baroclinic lows to tropical-like systems. *Weather Clim. Dynam.* **2021**, *2*, 255–279. [CrossRef]
14. Flaounas, E.; Raveh-Rubin, S.; Wernli, H.; Drobinski, P.; Bastin, S. The dynamical structure of intense Mediterranean cyclones. *Clim. Dyn.* **2015**, *44*, 2411–2427. [CrossRef]
15. Pytharoulis, I. Analysis of a Mediterranean tropical-like cyclone and its sensitivity to the sea surface temperatures. *Atmos. Res.* **2018**, *208*, 167–179. [CrossRef]
16. Miglietta, M.M.; Cerrai, D.; Laviola, S.; Cattani, E.; Levizzani, V. Potential vorticity patterns in Mediterranean "hurricanes". *Geophys. Res. Lett.* **2017**, *44*, 2537–2545. [CrossRef]
17. Portmann, R.; González-Alemán, J.J.; Sprenger, M.; Wernli, H. How an uncertain short-wave perturbation on the North Atlantic wave guide affects the forecast of an intense Mediterranean cyclone (Medicane Zorbas). *Weather Clim. Dyn.* **2020**, *1*, 597–615. [CrossRef]
18. Mazza, E.; Ulbrich, U.; Klein, R. The Tropical Transition of the October 1996 Medicane in the Western Mediterranean Sea: A Warm Seclusion Event. *Mon. Weather Rev.* **2017**, *145*, 2575–2595. [CrossRef]
19. Fita, L.; Flaounas, E. Medicanes as subtropical cyclones: The December 2005 case from the perspective of surface pressure tendency diagnostics and atmospheric water budget. *Q. J. R. Meteorol. Soc.* **2018**, *144*, 1028–1044. [CrossRef]
20. Shapiro, M.A.; Keyser, D. Fronts, jet streams and the tropopause. In *Extratropical Cyclones: The Erik Palmén Memorial Volume*; Newton, C.W., Holopainen, E.O., Eds.; American Meteorological Society: Boston, MA, USA, 1990; pp. 167–191. [CrossRef]
21. Schultz, D.M.; Vaughan, G. Occluded Fronts and the Occlusion Process: A Fresh Look at Conventional Wisdom. *Bull. Am. Meteorol. Soc.* **2011**, *92*, 443–466. [CrossRef]
22. Browning, K.A. Organization of clouds and precipitation in extratropical cyclones. In *Extratropical Cyclones: The Erik Palmén Memorial Volume*; Newton, C.W., Holopainen, E.O., Eds.; American Meteorological Society: Boston, MA, USA, 1990; pp. 129–153. [CrossRef]
23. Joos, H.; Wernli, H. Influence of microphysical processes on the potential vorticity development in a warm conveyor belt: A case-study with the limited-area model COSMO. *Q. J. R. Meteorol. Soc.* **2012**, *138*, 407–418. [CrossRef]
24. Wernli, H.; Joos, H.; Boettcher, M.; Madonna, E.; Pfahl, S. Warm Conveyor Belts in the ERA-Interim Dataset (1979–2010). Part II: Moisture Origin and Relevance for Precipitation. *J. Clim.* **2014**, *27*, 27–40. [CrossRef]
25. Bader, M.J.; Forbes, G.S.; Grant, J.R.; Lilley, R.B.E.; Waters, A. *Images in Weather Forecasting. A Practical Guide for Interpreting Satellite and Radar Imagery*; Cambridge University Press: Cambridge, UK, 1995.
26. Binder, H.; Boettcher, M.; Joos, H.; Wernli, H. The Role of Warm Conveyor Belts for the Intensification of Extratropical Cyclones in Northern Hemisphere Winter. *J. Atmos. Sci.* **2016**, *73*, 3997–4020. [CrossRef]
27. Sanders, F.; Gyakum, J.R. Synoptic-Dynamic Climatology of the "Bomb". *Mon. Weather Rev.* **1980**, *108*, 1589–1606. [CrossRef]
28. Lim, E.-P.; Simmonds, I. Explosive Cyclone Development in the Southern Hemisphere and a Comparison with Northern Hemisphere Events. *Mon. Weather Rev.* **2002**, *130*, 2188–2209. [CrossRef]
29. Kouroutzoglou, J.; Flocas, H.A.; Hatzaki, M.; Keay, K.; Simmonds, I.; Mavroudis, A. On the dynamics of a case study of explosive cyclogenesis in the Mediterranean. *Meteorol. Atmos. Phys.* **2015**, *127*, 49–73. [CrossRef]

30. Kouroutzoglou, J.; Avgoustoglou, E.N.; Flocas, H.A.; Hatzaki, M.; Skrimizeas, P.; Keay, K. Assessment of the role of sea surface fluxes on eastern Mediterranean explosive cyclogenesis with the aid of the limited-area model COSMO.GR. *Atmos. Res.* **2018**, *208*, 132–147. [CrossRef]

31. Cioni, G.; Malguzzi, P.; Buzzi, A. Thermal structure and dynamical precursor of a Mediterranean tropical-like cyclone. *Q. J. R. Meteorol. Soc.* **2016**, *142*, 1757–1766. [CrossRef]

32. Dee, D.P.; Uppala, S.M.; Simmons, A.J.; Berrisford, P.; Poli, P.; Kobayashi, S.; Andrae, U.; Balmaseda, M.A.; Balsamo, G.; Bauer, P.; et al. The ERA-Interim reanalysis: Configuration and performance of the data assimilation system. *Q. J. R. Meteorol. Soc.* **2011**, *137*, 553–597. [CrossRef]

33. Prezerakos, N.G.; Flocas, H.A. The role of a developing upper diffluent trough in surface cyclogenesis over central Mediterranean. *Meteorol. Z.* **1997**, *6*, 108–119. [CrossRef]

34. Prezerakos, N.G.; Flocas, H.A.; Michaelides, S.C. Upper-tropospheric downstream development leading to surface cyclogenesis in the central Mediterranean. *Meteorol. Appl.* **1999**, *6*, 313–322. [CrossRef]

35. Capaldo, M.; Conte, M.; Finizio, C.; Todisco, G. A Detailed Analysis of a Severe Storm in the Central Mediterranean—The Case of the Trapani Flood. *Riv. Di Meteorol. Aeronaut.* **1980**, *40*, 183–199.

36. Roebber, P.J. On the Statistical Analysis of Cyclone Deepening Rates. *Mon. Weather Rev.* **1989**, *117*, 2293–2298. [CrossRef]

37. Hart, R.E. A Cyclone Phase Space Derived from Thermal Wind and Thermal Asymmetry. *Mon. Weather Rev.* **2003**, *131*, 585–616. [CrossRef]

38. Pytharoulis, I.; Matsangouras, I.T.; Tegoulias, I.; Kotsopoulos, S.; Karacostas, T.S.; Nastos, P.T. *Numerical Study of the Medicane of November 2014*; Karacostas, T., Bais, A., Nastos, P.T., Eds.; Springer International Publishing: Cham, Switzerland, 2017; pp. 115–121.

39. Mylonas, M.; Douvis, K.; Polychroni, I.; Politi, N.; Nastos, P. Analysis of a Mediterranean Tropical-Like Cyclone. Sensitivity to WRF Parameterizations and Horizontal Resolution. *Atmosphere* **2019**, *10*, 425. [CrossRef]

40. Chaboureau, J.P.; Pantillon, F.; Lambert, D.; Richard, E.; Claud, C. Tropical transition of a Mediterranean storm by jet crossing. *Q. J. R. Meteorol. Soc.* **2012**, *138*, 596–611. [CrossRef]

41. Trenberth, K.E. On the Interpretation of the Diagnostic Quasi-Geostrophic Omega Equation. *Mon. Weather Rev.* **1978**, *106*, 131–137. [CrossRef]

42. Hoskins, B.J.; Draghici, I.; Davies, H.C. A new look at the ω-equation. *Q. J. R. Meteorol. Soc.* **1978**, *104*, 31–38. [CrossRef]

43. Thorncroft, C.D.; Hoskins, B.J. Frontal Cyclogenesis. *J. Atmos. Sci.* **1990**, *47*, 2317–2336. [CrossRef]

44. Davis, C.A.; Emanuel, K.A. Observational Evidence for the Influence of Surface Heat Fluxes on Rapid Maritime Cyclogenesis. *Mon. Weather Rev.* **1988**, *116*, 2649–2659. [CrossRef]

45. Carlson, T.N. Airflow Through Midlatitude Cyclones and the Comma Cloud Pattern. *Mon. Weather Rev.* **1980**, *108*, 1498–1509. [CrossRef]

46. Schultz, D.M. Reexamining the Cold Conveyor Belt. *Mon. Weather Rev.* **2001**, *129*, 2205–2225. [CrossRef]

47. Browning, K.A. Conceptual Models of Precipitation Systems. *Weather Forecast.* **1986**, *1*, 23–41. [CrossRef]

48. Semple, A.T. A review and unification of conceptual models of cyclogenesis. *Meteorol. Appl.* **2003**, *10*, 39–59. [CrossRef]

49. Gray, S.L.; Dacre, H.F. Classifying dynamical forcing mechanisms using a climatology of extratropical cyclones. *Q. J. R. Meteorol. Soc.* **2006**, *132*, 1119–1137. [CrossRef]

50. Prezerakos, N.G.; Flocas, H.A. The formation of a dynamically unstable ridge at 500 hPa as a precursor of surface cyclogenesis in the central Mediterranean. *Meteorol. Appl.* **2007**, *3*, 101–111. [CrossRef]

51. Kurz, M. *Training Guidelines of the German Meteorological Service*; German Meteorological Service: Offenbach am Main, Germany, 1998.